Nonlinear Dyn (2010) 62: 821–840
DOI 10.1007/s11071-010-9765-8

ORIGINAL PAPER

Order reduction of forced nonlinear systems using updated LELSM modes with new Ritz vectors

Mohammad A. AL-Shudeifat · Eric A. Butcher

Received: 21 November 2009 / Accepted: 13 June 2010 / Published online: 11 July 2010
© Springer Science+Business Media B.V. 2010

Abstract Enhanced modal-based order reduction of forced structural dynamic systems with isolated nonlinearities has been performed using the updated LELSM (local equivalent linear stiffness method) modes and new Ritz vectors. The updated LELSM modes have been found via iteration of the modes of the mass normalized local equivalent linear stiffness matrix of the nonlinear systems. The optimal basis vector of principal orthogonal modes (POMs) is found via simulation and used for POD-based order reduction for comparison. Two new Ritz vectors are defined as static load vectors. One of them gives a static displacement to the mass connected to the periodic forcing load and the other gives a static displacement to the mass connected to the nonlinear element. It is found that the use of these vectors, which are augmented to the updated LELSM modes in the order reduction modal matrix, reduces the number of modes used in order reduction and considerably enhances the accuracy of the order reduction. The combination of the new Ritz vectors with the updated LELSM modes in the order reduction matrix yields more accurate reduced models than POD-based order reduction of the forced nonlinear systems. Hence, the LELSM modal-based order reduction is enhanced via new Ritz vectors when compared with POD-based and linear-based order reductions. In addition, the main advantage of using the updated LELSM modes for order reduction is that, unlike POMs, they do not require a priori simulation and thus they can be combined with new Ritz vectors and applied directly to the system.

Keywords Nonlinear dynamic systems · Model order reduction · Local equivalent linear stiffness · Smooth nonlinearity · Proper orthogonal decomposition

M.A. AL-Shudeifat (✉) · E.A. Butcher
Department of Mechanical and Aerospace Engineering, New Mexico State University, Las Cruces, NM 88003, USA
e-mail: shdefat@nmsu.edu

1 Introduction

Various methods have been employed in approximating the response of n-dimensional linear and nonlinear dynamic systems by an $m(\ll n)$ dimensional dynamic system. The classical method for order reduction of linear systems is due to Guyan [1]. Extensions of Guyan reduction have been proposed that include inertial as well as stiffness effects in the order reduction transformation [2]. These linear-based Guyan-like order reduction techniques have also been applied to nonlinear dynamic systems with weak static and damping nonlinearities [3–6].

Another method for order reduction is the invariant manifold approach that has been used in reducing the dimension of the nonlinear dynamic systems to a reduced subspace of coordinates. It utilizes the nonlinear normal modes (NNMs) that describe the nonlinear motion of the system on a two-dimensional invariant

manifold in the system phase space [7–10]. As a result, the NNM-based reduced models are obtained in a subspace of the master coordinates [11, 12]. However, the NNM-based reduced models become less accurate than the linear-based reduced models at the internal resonance condition. The results of the frequency–amplitude dependence in [4] showed that the NNM-based reduced models were less accurate than the linear-based reduced models of the nonlinear systems with smooth nonlinearities for a range of parameters in the vicinity of an internal resonance condition. The invariant manifold approach was also employed in time-periodic systems [13] in which the use was made of the Liapunov–Floquet transformation [14].

Principal orthogonal decomposition (POD) is also a well-known technique that is used in modal analysis of nonlinear structural systems [15–22]. POD-based order reduction requires a priori simulation to form a subset of the dominant proper orthogonal modes (POMs) of the highest singular values. These optimal bases form the columns of the POD-based order reduction transformation matrix. The technique was applied for order reduction of structural systems with frictional excitation in [19] and for nonlinear dynamic systems with smooth and non-smooth nonlinearities in [20–22]. The POD-based reduced model was considerably enhanced via augmentation of the optimal bases of the POMs with a new type of Ritz vector called Kumar–Burton or K–B vectors in [22] for dynamic systems with coupling nonlinearities. The Ritz vector approach has also been applied in [23] in which a single Ritz vector was employed for each isolated nonlinearity along with a subset of linear basis functions to obtain a more accurate reduced model than that obtained only with the linear functions. However, the use of Ritz vectors in enhancing the accuracy of order reduction of dynamic systems is not a new topic. The approach was previously applied in order reduction of linear forced dynamic systems [24, 25]. The optimal Ritz vectors were augmented to a truncated subset of eigenvectors of the modal matrix of the linear system to form the order reduction transformation matrix. The load-dependent Ritz vectors were found by assigning a spatial distribution of the dynamic load to each substructure of the system [26, 27].

Another method that was developed for order reduction of linear structures by Hurty [28] and modified by Craig and Bampton in [29] has been extended to be used for order reduction of structures that have nonlinear components in [30]. In this study, the fixed-interface component mode synthesis (CMS) was extended for producing a reduced order model through utilizing the fixed-interface nonlinear normal modes (NNMs). In [31], the effect of a non-smooth nonlinearity that appears due to friction element in a structure with a friction-based seismic base isolation system was considered and added to the linear Craig–Bampton reduced equations of motion.

Most recently, a new technique for order reduction of dynamic systems with static piecewise linear nonlinearities was proposed based on previously developed methods for approximation of the NNM frequencies and mode shapes via either an amplitude-independent piecewise modal method (PMM) or an amplitude-dependent local equivalent linear stiffness method (LELSM) [6, 32, 33]. The technique was further improved over the previously developed methods for order reduction of large degree-of-freedom unforced nonlinear systems with grounded nonlinearities via iteration of the LELSM modes. The iterated LELSM modes were found to be a good approximation to the POMs of the system. These updated LELSM modes were found to be as efficient as POMs in the order reduction of such systems [33].

The LELSM modal-based order reduction via updated LELSM modes is enhanced in this study by using a new type of Ritz vector: the Sh-B vector. This approach is applied to forced dynamic systems with static grounded and coupling nonlinearities. The new Sh-B vectors are augmented to the updated LELSM order reduction matrix for such systems. These vectors considerably enhance the order reduction of these systems over the POD-based and linear-based order reductions.

2 Principal orthogonal decomposition

Consider the forced and damped n-degrees of freedom dynamic system with static nonlinearity as shown in Fig. 1 for which the equations of motion can be written as

$$M\ddot{x} + C\dot{x} + Kx + F_{\mathrm{nl}}(x) = F(t), \tag{1}$$

where $x \in \mathbf{R}^n$ is the vector of displacements, M is the $n \times n$ mass matrix, K is the $n \times n$ stiffness matrix, C is the $n \times n$ damping matrix, $F_{\mathrm{nl}}(x) =$

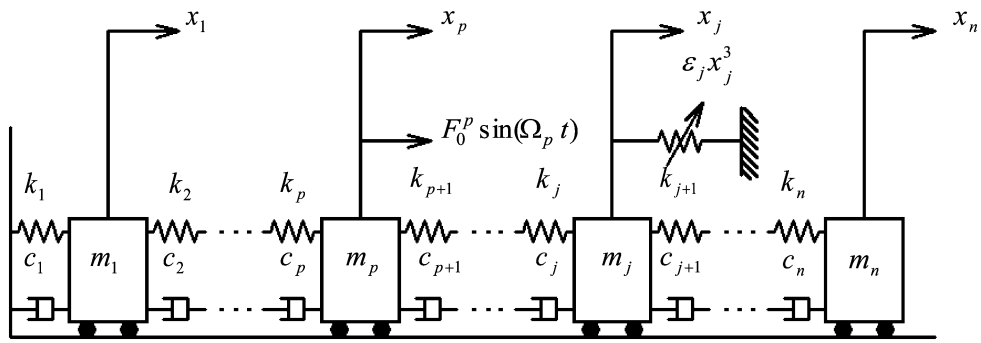

Fig. 1 n-degrees-of-freedom spring–mass system with forcing and one cubic spring

$[0 \ \ldots \ 0 \ f_{\text{nl}}^j(x_j) \ 0 \ \ldots \ 0]^{\text{T}}$ is the nonlinear $n \times 1$ force vector which for $1 \leq j \leq n$ consists of grounded static nonlinearities at jth degree-of-freedom, and $F(t) = [0 \ \ldots \ 0 \ F_0^p \ \sin(\Omega_p t) \ 0 \ \ldots \ 0]^{\text{T}}$ is the $n \times 1$ periodic excitation force vector that acts on mass p for $1 \leq p \leq n$.

The method of proper orthogonal decomposition (POD) requires a priori simulation of the dynamic system in (1) in space and time. The solution at m time steps is written in matrix form as [20]

$$X = [x_1 \quad x_2 \quad \ldots \quad x_n] = \begin{bmatrix} x_{11} & \ldots & x_{1n} \\ \vdots & \ddots & \vdots \\ x_{m1} & \ldots & x_{mn} \end{bmatrix}. \quad (2)$$

The covariance matrix X is centralized to the mean of data before applying the singular-value decomposition (SVD). The SVD is used for determining the POMs and the singular values σ_i^2 of the system. For the $m \times n$ matrix X in (2) the SVD can be written as [20]

$$X = USV^{\text{T}}, \quad (3)$$

where the POMs are the column vectors of the matrix V and the diagonal elements of matrix S are the singular values of the system. The subset of POMs that correspond to the higher singular values are selected to form the order reduction modal matrix, which physically means including the POMs with the greatest amount of energy in the signal. The ratio of energy in the first m POMs of highest singular values to the total energy of the n POMs is given by [20]

$$R_{\text{POD}} = \frac{\sum_{i=1}^{m} \sigma_i^2}{\sum_{i=1}^{n} \sigma_i^2}, \quad (4)$$

where σ_i^2 is the singular value corresponding to the mode i and $\sigma_1^2 > \sigma_2^2 > \cdots > \sigma_n^2$.

3 Local equivalent linear stiffness method

The local equivalent linear stiffness method (LELSM) has been previously utilized in [6] and [32, 33]. This method is used here for finding the local equivalent linear stiffnesses of the nonlinear springs. Finding such local equivalent stiffnesses yields the local equivalent linear stiffness matrix K_{eq} for the undamped and unforced nonlinear dynamic system. It is desired to find a local equivalent linear stiffness to the nonlinear spring attached to the jth degree-of-freedom. If $F(t) = 0$ and the nonlinear force $F_{\text{nl}}(x)$ in (1) acts on the jth degree-of-freedom, then the undamped equation of motion of the mass m_j in Fig. 1 is given as

$$m_j \ddot{x}_j + (k_j + k_{j+1})x_j + \varepsilon_j x_j^3 - k_j x_{j-1} - k_{j+1} x_{j+1} = 0. \quad (5)$$

The LELSM requires setting the coordinates of degrees-of-freedom $j-1$ and $j+1$ to zero, which yields the single degree-of-freedom system as shown in Fig. 2a. The equation of motion of this system is given as

$$m_j \ddot{x}_j + (k_j + k_{j+1})x_j + \varepsilon_j x_j^3 = 0. \quad (6)$$

Equation (6) can be rewritten as

$$\ddot{x}_j + \omega_j^2 \left(x_j + \frac{\beta_j \varepsilon_j}{\omega_j^2} x_j^3 \right) = 0, \quad (7)$$

where $\omega_j^2 = \sqrt{\frac{k_j + k_{j+1}}{m_j}}$ and $\beta_j = 1$.

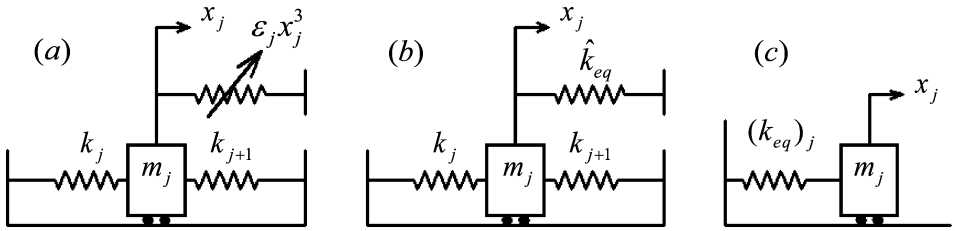

Fig. 2 (**a**) The single degree-of-freedom nonlinear spring–mass system, (**b**) and (**c**) local equivalent linear systems of the nonlinear system in (**a**)

An approximation for the nonlinear frequency in (7) was found via harmonic balance method in [34] to be

$$\begin{aligned}(k_{\text{eq}})_j &= m_j \Omega_j^2 \\ &= m_j \frac{\omega_j^2}{144}\left(80 + 62\left(\frac{\beta_j \varepsilon_j}{\omega_j^2}\right)X_j^2 \right. \\ &\quad \left. + \sqrt{4096 + 5888\left(\frac{\beta_j \varepsilon_j}{\omega_j^2}\right)X_j^2 + 1684\left(\frac{\beta_j \varepsilon_j}{\omega_j^2}\right)^2 X_j^4}\right),\end{aligned} \tag{8}$$

where j is the degree-of-freedom location and X_j is the initial modal amplitude for that degree-of-freedom.

The equations of motions of the local equivalent linear systems in Fig. 2b and c, respectively, are given as

$$m_j \ddot{x}_j + (k_j + k_{j+1} + \hat{k}_{\text{eq}})x_j = 0, \tag{9}$$

$$m_j \ddot{x}_j + (k_{\text{eq}})_j x_j \equiv 0, \tag{10}$$

where $k_j + k_{j+1} + \hat{k}_{\text{eq}} = (k_{\text{eq}})_j = m_j \Omega_j^2$ and Ω_j^2 is given in (8). Hence, the nonlinear equation of motion of m_j is rewritten in its equivalent linear form as

$$m_j \ddot{x}_j + (k_{\text{eq}})_j x_j - k_j x_{j-1} - k_{j+1} x_{j+1} = 0. \tag{11}$$

The updated stiffness matrix is therefore given by

$$K_{\text{eq}} = \begin{bmatrix} 2 & -1 & & & & & \\ -1 & 2 & -1 & & & 0 & \\ & \ddots & \ddots & \ddots & & & \\ & & -1 & (k_{\text{eq}})_j & -1 & & \\ & & & \ddots & \ddots & \ddots & \\ & 0 & & & -1 & 2 & -1 \\ & & & & & -1 & 1 \end{bmatrix}. \tag{12}$$

The updated global stiffness matrix in (12) is symmetric, therefore yielding orthogonal LELSM modes. This stiffness matrix is normalized as $\tilde{K}_{\text{eq}} = M^{-1/2} K_{\text{eq}} M^{-1/2}$ and the eigenvalue problem $|\tilde{K}_{\text{eq}} - \Omega^2 I|x = 0$ yields the LELSM modes and their frequencies. In the following, the LELSM methodology is modified by updating the LELSM modes. If the n-degrees-of-freedom system has the jth degree-of-freedom attached to a nonlinear spring then the updated LELSM modes are found via the following iteration technique [33]:

1. Use arbitrary initial amplitude for $x_j^{(1)}(0)$ or let $x_j^{(1)}(0) = \phi_{j1}$ where ϕ_{j1} is the jth element of the first linear mode of the system.
2. At $k = 1$ and $x_j^{(1)}(0)$, find $(k_{\text{eq}})_j$ to form $(K_{\text{eq}})_{n\times n}$, then solve for the first LELSM mode shape $\tilde{\phi}_1^{(1)}$ to get $\tilde{\phi}_{j1}^{(1)}$.
3. At $k = 2$, set $x_j^{(2)}(0) = \frac{(\tilde{\phi}_{j1}^{(1)} + x_j^{(1)}(0))}{2}$ and solve for $\tilde{\phi}_1^{(2)}$ to get $\tilde{\phi}_{j1}^{(2)}$.
4. For each new value of $x_j^{(k)}(0)$, find $(k_{\text{eq}})_j$ to form $(K_{\text{eq}})_{n\times n}$ and solve for a new $\tilde{\phi}_1^{(k)}$ to get new value of $\tilde{\phi}_{j1}^{(k)}$.
5. Continue iteration up to $k = m$, then set $x_j^{(m)}(0) = \frac{(\phi_{j1}^{(m-1)} + x_j^{(m-1)}(0))}{2}$ and solve for $\tilde{\phi}_1^{(m)}$. If $\tilde{\phi}_1^{(m)} - \tilde{\phi}_1^{(m-1)} \leq e$, then stop. Otherwise continue iteration until the LELSM mode converges to a unique shape. Hence, the updated LELSM modes are obtained.

It is found that the POMs obtained by using the first linear mode as the initial condition for the unforced nonlinear system are well-approximated by the updated LELSM modes [33]. Figure 3 shows a comparison between the first POM and the first updated LELSM mode for the undamped unforced nonlinear

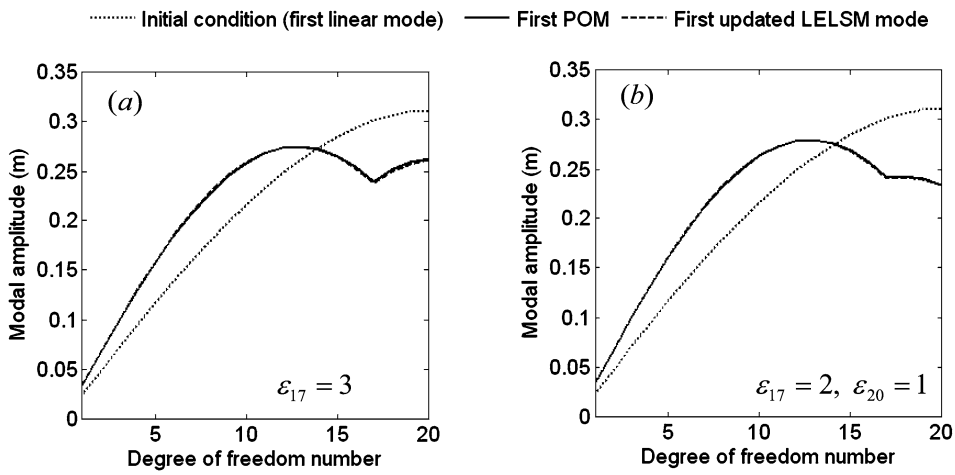

Fig. 3 Comparison between the first POM and the first updated LELSM mode for the nonlinear spring–mass system: (**a**) one cubic spring of $\varepsilon_{17} = 3$ is attached to m_{17}, (**b**) two cubic springs of $\varepsilon_{17} = 2$ and $\varepsilon_{20} = 1$ are attached to m_{17} and m_{20}, respectively

20-degrees-of-freedom spring–mass system when the first linear mode (also shown with the dotted line) is used as the initial condition. The almost indistinguishable overlap between the first POM and the first updated LELSM mode is clearly noticed in the figure.

The high degree of similarity between the POMs and the updated LELSM modes is also verified using the Euclidean angle $\cos(\theta_i)$ and the static mode energy difference $(\Delta E)_i$ between the updated LELSM modes and the corresponding POMs. The ith POM ($\hat{\phi}_i$) and updated LELSM ($\tilde{\phi}_i$) modes are compared via the Euclidean angle $\cos(\theta_i(\hat{\phi}_i, \tilde{\phi}_i))$ and the static mode energy difference $(\Delta E)_i$ when the ith linear mode ϕ_i is used as the initial condition:

$$\left((\Delta E)_i = \tilde{\phi}_i^{\mathrm{T}} K_{\mathrm{eq}} \tilde{\phi}_i - \hat{\phi}_i^{\mathrm{T}} K_{\mathrm{eq}} \hat{\phi}_i\right) \to 0 \quad \text{(minimum)}, \tag{13a}$$

$$\left(\cos\left(\theta_i(\hat{\phi}_i, \tilde{\phi}_i)\right) = \tilde{\phi}_i^{\mathrm{T}} \hat{\phi}_i / \left(\left\|\tilde{\phi}_i^{\mathrm{T}} \tilde{\phi}\right\| \left\|\hat{\phi}_i^{\mathrm{T}} \hat{\phi}_i\right\|\right)\right) \to 1 \quad \text{(maximum)}. \tag{13b}$$

The angle $\theta_i(\hat{\phi}_i, \tilde{\phi}_i)$ and the energy difference $(\Delta E)_i$ are calculated for the example in Fig. 3b and given in Table 1. It is shown that these quantities are within 3 or 4 significant digits of their optimal values. Hence, the near optimality of the updated LELSM modes is verified when compared with POMs, which are themselves optimal with respect to energy content.

Furthermore, the updated LELSM modes $\tilde{\Phi} = \{\tilde{\phi}_1, \tilde{\phi}_2, \ldots, \tilde{\phi}_n\}$ span the space $D \in \mathbf{R}^{n \times n}$ that is spanned by the dominant POMs $\hat{\Phi} = \{\hat{\phi}_1, \hat{\phi}_2, \ldots, \hat{\phi}_n\}$, i.e., $D = \mathrm{span}(\hat{\phi}_1, \hat{\phi}_2, \ldots, \hat{\phi}_n)$. More specifically, there exist a set of real vectors $v_i = \tilde{\Phi}^{\mathrm{T}} \hat{\phi}_i, i = 1, 2, \ldots, n$, such that the ith POM is calculated as $\hat{\phi}_i = \tilde{\Phi} v_i$ where $R_i = \|\tilde{\Phi} v_i - \hat{\phi}_i\| \to 0$. Therefore, the space spanned by the dominant POMs can be closely approximated by a linear combination of the updated LELSM modes.

For the example in Fig. 3b, the residual R_i is plotted in Fig. 4a where $|R_i| < 3 \times 10^{-30}$ for $i = 1, 2, \ldots, n$. Hence, the updated LELSM modes form a basis that spans the space defined by the dominant POMs while all POMs can be represented by a linear combination of the updated LELSM modes.

Beside the close approximation of the POMs via the updated LELSM modes discussed above, another type of comparison can be made from the frequencies of the updated LELSM modes. It is shown that when the first linear mode is utilized as the initial condition for the unforced nonlinear 20-degrees-of-freedom spring–mass system, the exact frequency of the full model obtained via numerical simulation is found to be well approximated by the first updated LELSM mode frequency as shown in Fig. 4b. Otherwise, the frequency of the LELSM mode before updating is not an accurate approximation for the exact frequency of the nonlinear system. It is shown here that the updated LELSM modes and their frequencies are an efficient approximation for describing the modal behavior of the nonlinear dynamic systems considered here. This

Table 1 Euclidean angle $\cos(\theta_i(\hat{\phi}_i, \tilde{\phi}_i))$and the energy difference $(\Delta E)_i$ between the updated LELSM modes and the corresponding POMs for the first 6 modes

	1st mode	2nd mode	3rd mode	4th mode	5th mode	6th mode
$\cos(\theta_i(\hat{\phi}_i, \tilde{\phi}_i))$	1.0000	0.9962	0.9926	0.9994	0.9999	0.9992
$\tilde{\phi}_i K_{\text{eq}} \tilde{\phi}_i$	0.0153	0.0620	0.1497	0.2851	0.4647	0.6806
$\hat{\phi}_i K_{\text{eq}} \hat{\phi}_i$	0.0153	0.0621	0.1500	0.2850	0.4647	0.6807
$(\Delta E)_i$	1.3×10^{-6}	1.6×10^{-4}	2.6×10^{-4}	1.4×10^{-4}	4.9×10^{-5}	1.4×10^{-4}

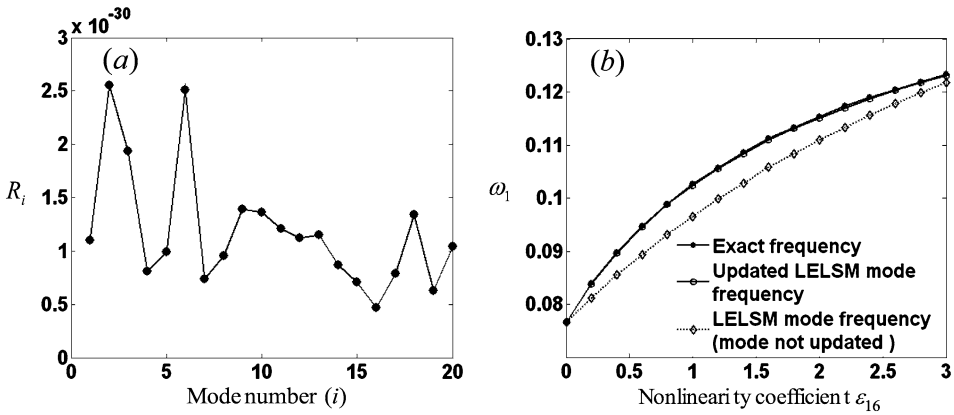

Fig. 4 (**a**) Residual $R_i = \|\tilde{\Phi} v_i - \hat{\phi}_i\|$ for the example of Fig. 3b, (**b**) approximation of the exact frequency of the first mode found via numerical simulation of the full model by the frequency of the first updated LELSM mode

can be quantified by the difference between the frequency content of the ith updated LELSM mode from the frequency content of the ith linear mode as

$$\delta_i = (\omega_i)_{\text{LELSM}} - (\omega_i)_{\text{Linear}}, \tag{14}$$

where $(\omega_i)_{\text{LELSM}}$ is the ith updated LELSM mode frequency and $(\omega_i)_{\text{Linear}}$ is ith linear mode frequency. For $(\omega_i)_{\text{LELSM}} = (\omega_i)_{\text{Linear}}$, both updated LELSM and linear modes are similar where $\delta_i = 0$. The percent deviation in the frequency content between the updated LELSM modes and the corresponding linear modes is quantified as

$$R_{\text{LELSM}} = \frac{\sum_{i=1}^{m} |\delta_i|}{\sum_{i=1}^{n} |\delta_i|}. \tag{15}$$

The percent deviation in the frequency content R_{LELSM} is used as a criterion to predefine the number of modes that gives a reduced model which is comparable in accuracy to the full model. This will be shown later in the examples that are considered in this paper.

4 New Ritz vectors for order reduction

The updated LELSM modes have been found as efficient as POMs in reducing the order of the damped unforced nonlinear dynamic systems with static nonlinearities [33]. The use of the updated LELSM modes in reducing the order of such systems with periodic forcing excitation, such as the system in Fig. 1, is greatly aided through the simultaneous use of new Ritz vectors that enhance the order reduction. These Ritz vectors should have appropriate discontinuities at the forcing and the nonlinearity locations. For this purpose, a subset of new Ritz vectors is suggested and augmented with the updated LELSM modes in the order reduction transformation matrix for a forced nonlinear dynamic system. The new static load Ritz vec-

tors are selected to be relevant to the nonlinear system in Fig. 1. These new vectors are proportional to the stiffnesses of the masses attached to the forcing or nonlinear springs. If the forcing acts on the pth degree-of-freedom and the nonlinear spring is attached to the jth degree-of-freedom, the first new static load Ritz vector is given as

$$R_1 = \alpha[0 \quad \dots \quad 0 \quad -k_p \quad k_p + k_{p+1} \quad -k_{p+1} \quad 0 \quad \dots \quad 0]^{\mathrm{T}} \tag{16}$$

while the other new static load Ritz vector is given as

$$R_2 = \alpha[0 \quad \dots \quad 0 \quad -k_j \quad (k_{\mathrm{eq}})_j \quad -k_{j+1} \quad 0 \quad \dots \quad 0]^{\mathrm{T}} \tag{17}$$

where $\alpha = 1\ \mathrm{m}^{-1}$ and R_1 and R_2 are of dimension $n \times 1$. The corresponding static displacement Ritz vectors are calculated as

$$r_1 = K_{\mathrm{eq}}^{-1} R_1, \tag{18a}$$

$$r_2 = K_{\mathrm{eq}}^{-1} R_2. \tag{18b}$$

This new type of Ritz vector is called an Sh-B vector. These vectors are linearly independent but not necessarily orthogonal to the updated LELSM vectors, and have appropriate discontinuities at the forcing and the nonlinearity locations. The augmentation of a conventional basis set (i.e. the updated LELSM modes) with these Sh-B vectors yields a basis that effectively captures the nature of the configuration space for the dynamic systems with localized nonlinearities and forcing. The Sh-B vectors capture the effect of the nonlinearity and forcing and couple this to the remainder of the coordinates, especially in the immediate vicinity of the nonlinearity and forcing locations. Hence, the augmentation of the updated LELSM modes with Sh-B vectors is expected to enhance the reduced order model for the forced nonlinear spring–mass system with grounded nonlinearities.

5 Modal-based order reduction

It is desired to reduce the order of the forced nonlinear n-degrees-of-freedom mass–spring system shown previously in Fig. 1 to an equivalent m-degrees-of-freedom system where $m \ll n$. Hence, the modal based order reduction requires forming an $n \times m$ transformation matrix Φ of the first m columns of the basis of the $n \times n$ modal matrix of the POD modes, LELSM modes or the linear modes of the system as

$$\Phi_{n\times m} = [\phi_1 \quad \phi_2 \quad \dots \quad \phi_m]. \tag{19}$$

To enhance the modal-based order reduction of the system with one forcing and one grounded cubic spring, the new Sh-B displacement vectors r_1 and r_2 are augmented to the order reduction modal matrix Φ, which yields the enhanced transformation matrix $\tilde{\Phi}$:

$$\tilde{\Phi}_{n\times m} = [\phi_1 \quad \phi_2 \quad \dots \quad \phi_{m-2} \quad r_1 \quad r_2]. \tag{20}$$

This enhanced order reduction transformation matrix is used to obtain an enhanced order reduction via Sh-B vectors. The order reduction is performed by applying the transformation $x_{n\times 1} = \tilde{\Phi}_{n\times m} z_{m\times 1}$ to (1) and premultiplying by $\tilde{\Phi}^{\mathrm{T}}$, which yields

$$\bar{M}\ddot{z} + \bar{C}\dot{z} + \bar{K}z + f_{\mathrm{nl}}(z) = f(t), \tag{21}$$

where $\tilde{\Phi}^{\mathrm{T}} M \tilde{\Phi} = \bar{M}, \tilde{\Phi}^{\mathrm{T}} C \tilde{\Phi} = \bar{C}, \tilde{\Phi}^{\mathrm{T}} K \tilde{\Phi} = \bar{K}$, $\hat{F}(z) = F_{\mathrm{nl}}(\tilde{\Phi} z)$, $f_{\mathrm{nl}}(z) = \tilde{\Phi}^{\mathrm{T}} \hat{F}(z)$, and $f(t) = \tilde{\Phi}^{\mathrm{T}} F(t)$.

The reduced $\bar{M}, \bar{C}$ and $\bar{K}$ matrices are all symmetric even though the Sh-B vectors are augmented to the order reduction modal matrix. The reduced model stiffness matrix is normalized as $\widehat{K} = \bar{M}^{-1/2} \bar{K} \bar{M}^{-1/2}$ where the eigenvalue problem $|\widehat{K} - (\Omega^2)_r I| x = 0$ yields the frequencies of the m modes of the reduced model where $m - 2$ of these frequencies are exactly the same as the first $m - 2$ frequencies of the updated LELSM modes. Hence, the augmentation of the Sh-B vectors does not affect the first $m - 2$ frequencies of updated LELSM modes in the reduced model.

6 Order reduction of forced, damped and nonlinear mass–spring systems

Three cases are considered to show the capability of the new Sh-B vectors in enhancing the LELSM-based order reduction of the forced nonlinear dynamic system. The initial condition for all cases is the first linear mode $x(0) = \phi_1$ for the displacements and $\dot{x}(0) = 0.1\phi_1$ for the velocities.

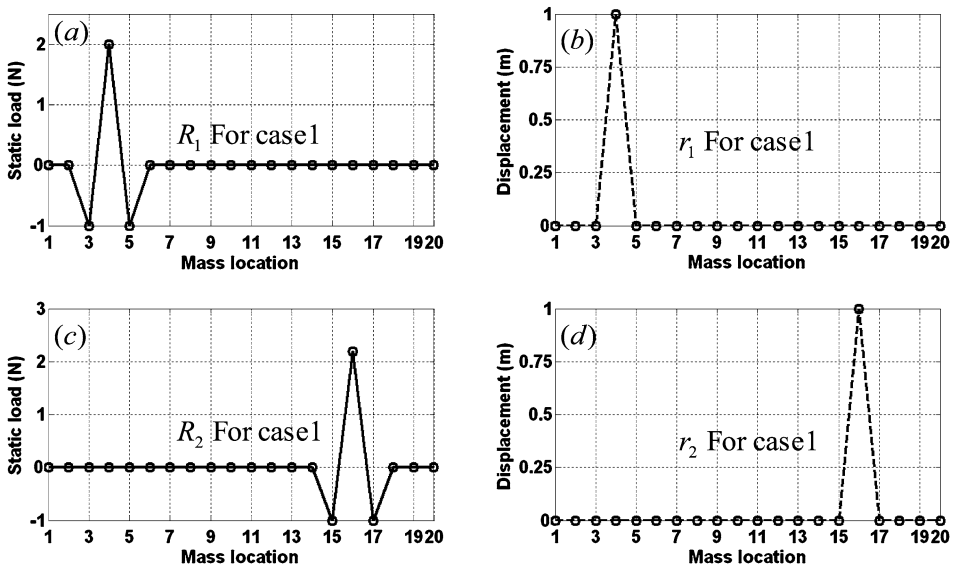

Fig. 5 Static load Sh-B vectors and their corresponding displacements of the masses of the 20-degrees-of-freedom spring–mass system with forcing excitation acting on m_4 and cubic spring attached to m_{16}

Case 1 For the forced, damped and nonlinear system in Fig. 1: all masses and stiffnesses are set to unity at an appropriate units, $n = 20$; the periodic excitation load amplitude is $F_0^4 = 3N$ which acts on mass m_4; the cubic spring is attached to mass m_{16} where $f_{\text{nl}}^{16}(x_{16}) = \varepsilon_{16} x_{16}^3$ for $\varepsilon_{16} = 3$; the forcing frequency Ω_4 is the average of the first three natural frequencies of the linear system, and the damping matrix is proportional to the stiffness matrix as $C = \gamma K$ where $\gamma = 0.04$. The first static load Sh-B vector R_1 displaces the forced mass m_4 by a unit displacement and keeps all other masses with zero displacements. The second static load Sh-B vector displaces m_{16} by a unit displacement and keeps all other masses with zero displacements. These static load and displacement Sh-B vectors are plotted in Fig. 5.

The phase plane portraits are plotted for m_{16} in Fig. 6 and the results of this figure are summarized in Table 2. It is shown that as the number of retained modes in the reduced models increases, the accuracy of the enhanced LELSM-based reduced model increases faster than that of the POD-reduced model. If the number of the retained modes in the POD-based reduced model is increased from 9 to 10, the R_{POD} changes from 0.9905 to 0.9931 as shown in Table 2, which does not actually reflect the considerable enhancement between the 9 POMs and 10 POMs reduced models. As a result, R_{POD} (which is known as a strong criterion for identifying the highest energy modes) is found here to not necessarily distinguish the minimum number of the retained modes to obtain a reduced order model of an acceptable accuracy. The criterion R_{LELSM} is found to be a more reliable criterion for predefining the necessary number of the retained modes that reflects the required accuracy in the reduced model than R_{POD} as shown in Table 2, which reflects the smooth enhancement in the LELSM-based reduced model as the number of the retained modes is increased as shown in Fig. 6. In addition, the calculation of the accumulated least square error between the simulations of the exact and the reduced models has shown that the LELSM-based reduced model is almost more accurate than both POD-based and linear-based reduced models as shown in Table 3.

The reduced models obtained via updated LELSM modes and two Sh-B vectors are shown in Fig. 7 for different values of the nonlinearity coefficients at fixed values of the forcing amplitude. In addition, Fig. 8 shows the reduced models of the system at fixed values of the nonlinearity coefficient for different values of the forcing amplitudes. Both figures show that the LELSM modal-based order reduction via updated LELSM modes and Sh-B vectors stays accurate for different values of either forcing amplitudes or nonlinearity coefficients.

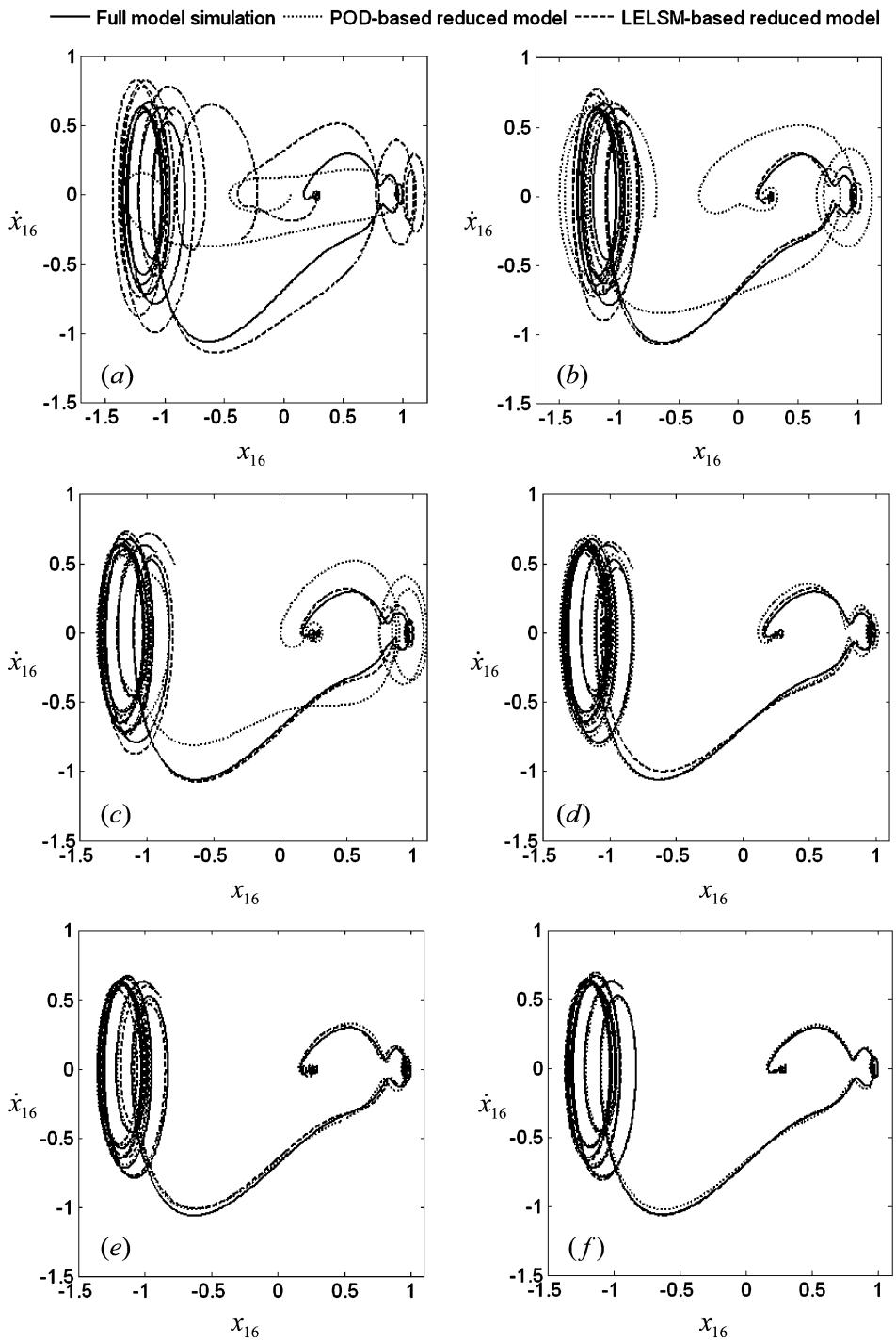

Fig. 6 Phase plane portraits obtained via simulation of the system in case 1 up to $t = 35$ s, where the number of modes retained in the reduced model is (**a**) 5, (**b**) 7, (**c**) 9, (**d**) 10, (**e**) 11, (**f**) 12

Case 2 A forced nonlinear 100-degrees-of-freedom spring–mass system ($n = 100$) is considered here. Two cubic springs of $\varepsilon_{30} = 3$ and $\varepsilon_{60} = 1$ are attached to the masses m_{30} and m_{60}, respectively, and a forc-

Table 2 Comparison between the POD-based and the LELSM-based reduced models

Figure No.	POD-based	R_{POD}	LELSM-based	R_{LELSM}
Fig. 6a	5 POMs	0.9722	3 updated LELSM modes + 2 Sh-B vectors	0.6810
Fig. 6b	7 POMs	0.9836	5 updated LELSM modes + 2 Sh-B vectors	0.7338
Fig. 6c	9 POMs	0.9905	7 updated LELSM modes + 2 Sh-B vectors	0.7854
Fig. 6d	10 POMs	0.9931	8 updated LELSM modes + 2 Sh-B vectors	0.8289
Fig. 6e	11 POMs	0.9953	9 updated LELSM modes + 2 Sh-B vectors	0.8435
Fig. 6f	12 POMs	0.9965	10 updated LELSM modes + 2 Sh-B vectors	0.8438

Table 3 Least square error between simulations of the full and reduced models for x_{16}

No. of modes retained	6	7	8	9	10	11	12
Accumulated least square error for 100 seconds simulation							
POD-based	1505.5	905.4	494	616.1	136.2	38.1	31.1
LELSM-based	558.7	512.6	312.1	362.1	34.2	32.3	6.95
Linear-based	828.4	561.2	392.7	405.9	37.2	35.7	7.34
Accumulated least square error for 500 seconds simulation							
POD-based	10143	5418.5	3584.1	3390.3	1103	420.3	353.2
LELSM-based	14592	5595	2181	1944.8	1204.1	515.3	108.2
Linear-based	14173	6241	2304	2097.6	1281.6	522.1	116.6

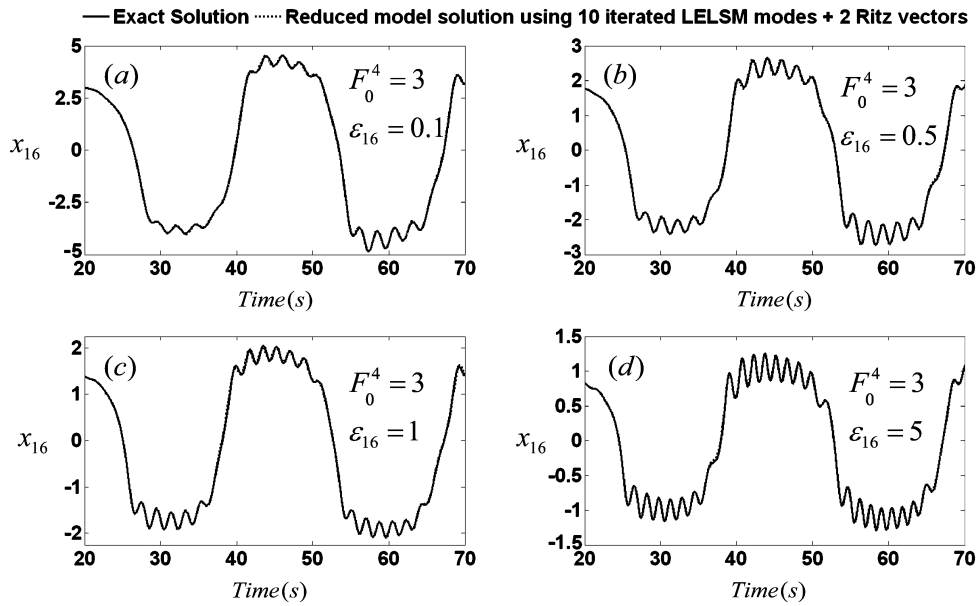

Fig. 7 Simulations of the 16th degree-of-freedom of the full model and its reduced models for different values of the nonlinearity coefficient ε for a fixed value of forcing amplitude F_0^4

ing of amplitude $F_0^{100} = 10$ N acts on the right-end mass m_{100}. The system is similar to that in Fig. 1, except that two cubic springs and one forcing location are used here. For this example, three static load Sh-B vectors are used with two of them (R_1, R_2) for the cubic nonlinearities and one (R_3) for the forcing. They

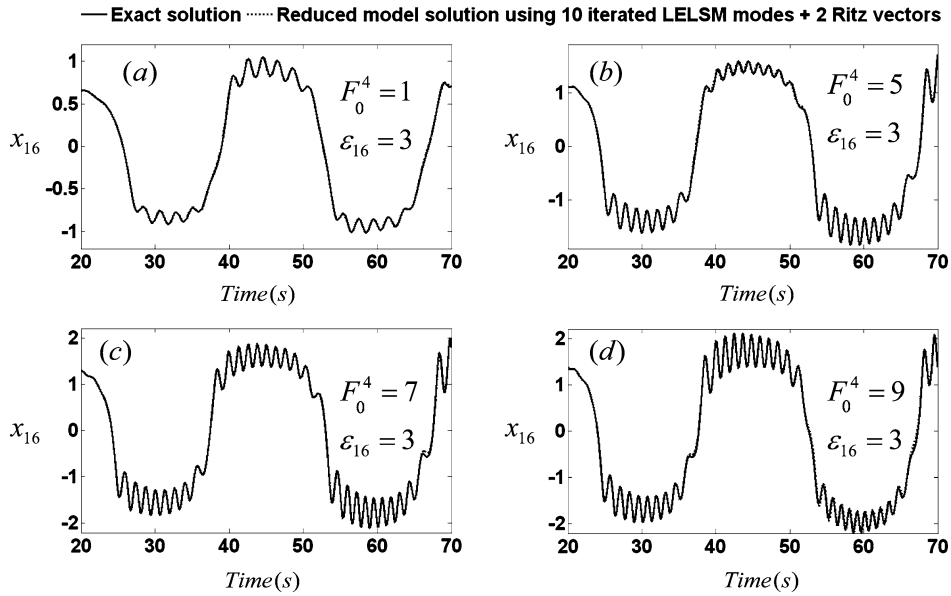

Fig. 8 Simulations of the 16th degree-of-freedom of the full model and its reduced models for different values of the forcing amplitudes F_0^4 at a fixed nonlinearity coefficient ε

are given for $\alpha = 1\ \mathrm{m}^{-1}$ as

$$R_1 = \alpha[0 \quad \ldots \quad 0 \quad -k_{30} \quad (k_{\mathrm{eq}})_{30} \quad -k_{31} \quad 0 \quad \ldots \quad 0]^{\mathrm{T}}, \tag{22a}$$

$$R_2 = \alpha[0 \quad \ldots \quad 0 \quad -k_{60} \quad (k_{\mathrm{eq}})_{60} \quad -k_{61} \quad 0 \quad \ldots \quad 0]^{\mathrm{T}}, \tag{22b}$$

$$R_3 = \alpha[0 \quad \ldots \quad 0 \quad -k_{100} \quad k_{100}]^{\mathrm{T}}. \tag{22c}$$

The forcing frequency is selected to be equal to the average of the first five linear mode frequencies and the damping matrix is proportional to the stiffness matrix as $C = \gamma K$ where $\gamma = 0.01$. The system is simulated up to 1000 s for finding the POMs where the initial condition is the first linear mode $x(0) = \phi_1$ for the displacements and $\dot{x}(0) = 0.1\phi_1$ for the velocities. The high degree of similarity between the first POM and the first updated LELSM mode of this system is shown in Fig. 9. The LELSM-based reduced models in Fig. 10 that result from the augmentation of the updated LELSM modes with three Sh-B vectors are found to be comparable to the POD-reducedreduced models in Fig. 11. In this example, the validity of using more than two Sh-B vectors is demonstrated. In addition, the least square error in Table 4 between the simulations of m_{100} displacement in the full and reduced models shows that the enhanced LELSM-based

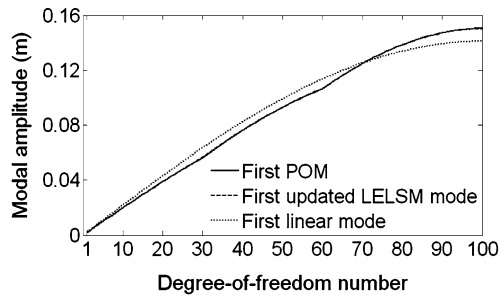

Fig. 9 Comparison between the first POM and the first updated LELSM modes for case 2

reduced model via Sh-B vectors is comparable in accuracy to the POD-based reduced model when 50 or 55 modes are retained in the reduced models. Similar conclusions are also observed for the other degrees-of-freedom in this example.

Case 3 In this case, a forced nonlinear 100-degrees-of-freedom spring–mass system ($n = 100$) is also considered, while the two cubic springs of $\varepsilon_{30} = 3$ and $\varepsilon_{100} = 1$ are attached to the masses m_{30} and m_{100}, respectively. For this case, the forcing of amplitude $F_0^{60} = 10$ acts on mass m_{60}. Three static load Sh-B vectors are used here where two of them (R_1, R_2) are used for cubic nonlinearities and one (R_3) is used for

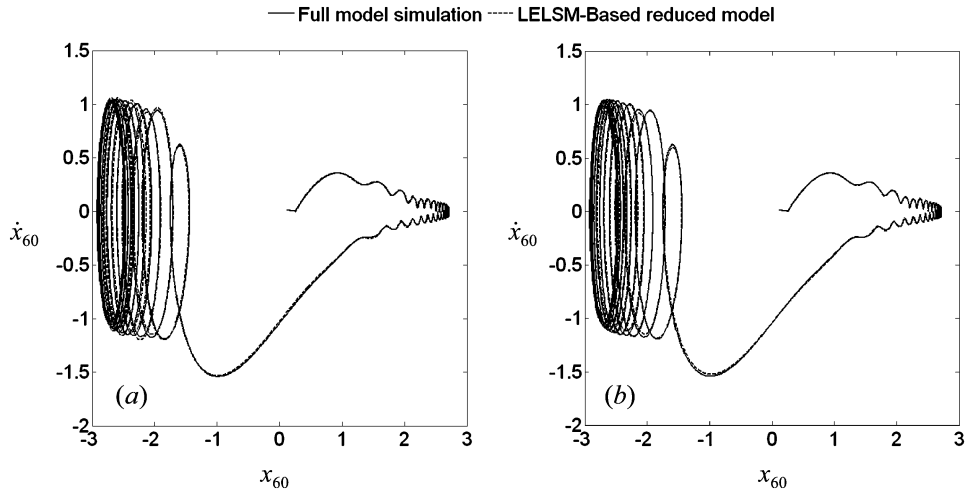

Fig. 10 Phase plane portraits of m_{60} obtained via numerical simulation of the full model and its reduced models up to $t = 100$ s: (**a**) 47 updated LELSM modes combined with three Sh-B vectors, (**b**) 52 updated LELSM modes combined with three Sh-B vectors

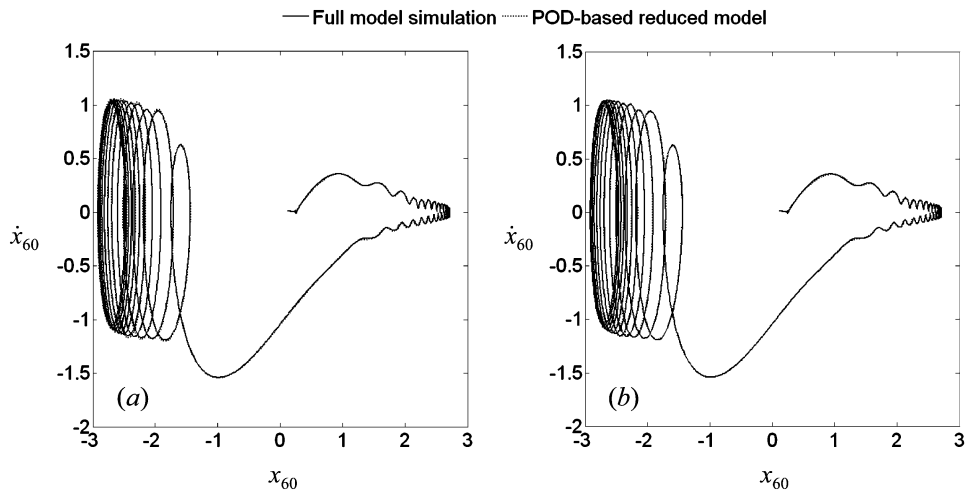

Fig. 11 Phase plane portraits of m_{60} obtained via numerical simulation of the full model and its reduced models up to $t = 100$ s : (**a**) 50 POMs, (**b**) 55 POMs

Table 4 Least square error '*LE*' between simulations of the full and reduced models for x_{60}

Simulation time	100 seconds				500 seconds
No. of modes retained	40	45	50	55	55
POD-based reduced model, $LE =$	149.54	15.07	0.299	0.122	420.5
LELSM-based reduced model, $LE =$	7.151	1.588	0.756	0.404	452.5
Linear-based reduced model, $LE =$	2.204	1.004	0.949	0.233	617.6
R_{POD}	0.9984	0.9988	0.9992	0.9994	0.9994
R_{LELSM}	0.8229	0.8420	0.8612	0.8771	0.8771

forcing. They are given for $\alpha = 1\ \mathrm{m}^{-1}$ as

$$R_1 = \alpha[0 \quad \ldots \quad 0 \quad -k_{30} \quad (k_{\mathrm{eq}})_{30} \quad -k_{31} \quad 0 \quad \ldots \quad 0]^{\mathrm{T}}, \tag{23a}$$

$$R_2 = \alpha[0 \quad \ldots \quad 0 \quad -k_{100} \quad (k_{\mathrm{eq}})_{100}]^{\mathrm{T}}, \tag{23b}$$

$$R_3 = \alpha[0 \quad \ldots \quad 0 \quad -k_{60} \quad k_{60}+k_{61} \quad -k_{61} \quad 0 \quad \ldots \quad 0]^{\mathrm{T}}. \tag{23c}$$

The forcing frequency and the damping matrix are selected to be similar to those in case 2. The system is simulated up to 1000 s for the same initial condition that was previously used in case 2. The high degree of similarity between the first POM and the first updated LELSM mode of this system is shown Fig. 12. Similarly to case 2, the LELSM-based reduced models in Fig. 13 that result from the augmentation of the updated LELSM modes with three Sh-B vectors are found to be comparable to the POD-reduced reduced models in Fig. 14 when 50 or 55 modes are retained in the reduced model. In this example, the least square error in Table 5 between the simulations of the full and the reduced models shows that the enhanced LELSM-based reduced model via Sh-B vectors is more accurate than both POD-based and the linear-based reduced models for 500 s of simulation. Furthermore, the augmentation of the Sh-B vectors with the linear modes in the order reduction modal matrix gives more accurate reduced model than the POD-based reduced model as shown in Table 5. Similar conclusions are drawn for the other degrees-of-freedom of this dynamic system.

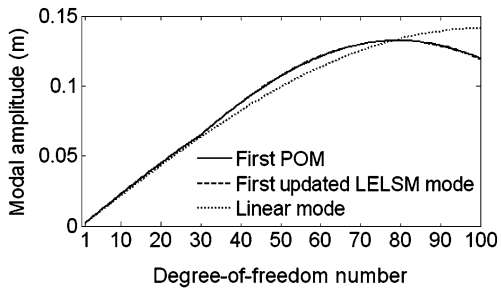

Fig. 12 Comparison between the first POM and the first updated LELSM modes for case 3

7 Order reduction of 20-dof mass–spring system with coupling nonlinearity

The forced system with coupling nonlinear spring is shown in Fig. 15. The coupling cubic nonlinear spring is attached between masses m_j and m_{j+1}. The equations of motion are the same as (1) except for the nonlinearity force vector which is given as $F_{\mathrm{nl}}(x) = [0 \ \ldots \ 0 \ f_{\mathrm{nl}}^{j}(x_j) \ f_{\mathrm{nl}}^{j+1}(x_{j+1}) \ 0 \ \ldots \ 0]^{\mathrm{T}}$ for $1 \le j \le n$ where $f_{\mathrm{nl}}^{j}(x_j) = \varepsilon_j (x_j - x_{j+1})^3$ and $f_{\mathrm{nl}}^{j+1}(x_{j+1}) = -\varepsilon_j (x_j - x_{j+1})^3$.

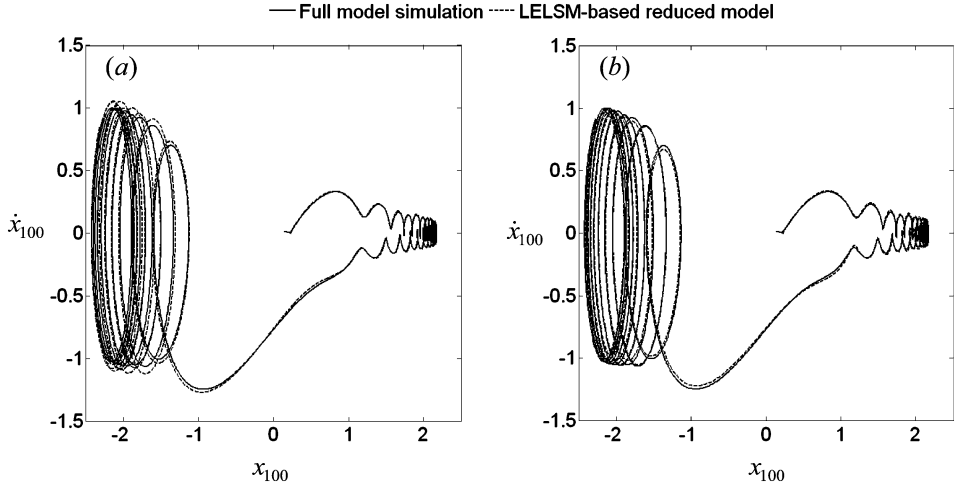

Fig. 13 Phase plane portraits of m_{60} obtained via numerical simulation of the full model and its reduced models up to $t = 100$ s: (**a**) 47 updated LELSM modes combined with three Sh-B vectors, (**b**) 52 updated LELSM modes combined with three Sh-B vectors

Table 5 Least square error '*LE*' between simulations of the full and reduced models for x_{100}

Simulation time	100 seconds				500 seconds
No. of modes retained	40	45	50	55	55
POD-based reduced model, $LE =$	2.1454	7.3397	3.3036	1.0455	2250.0
LELSM-based reduced model, $LE =$	2.5291	1.7293	1.8075	0.3501	1898.2
Linear-based reduced model, $LE =$	2.5225	1.7421	1.8115	0.3448	1955.9
R_{POD}	0.9979	0.9984	0.9988	0.9991	0.9991
R_{LELSM}	0.8946	0.9113	0.9267	0.9385	0.9385

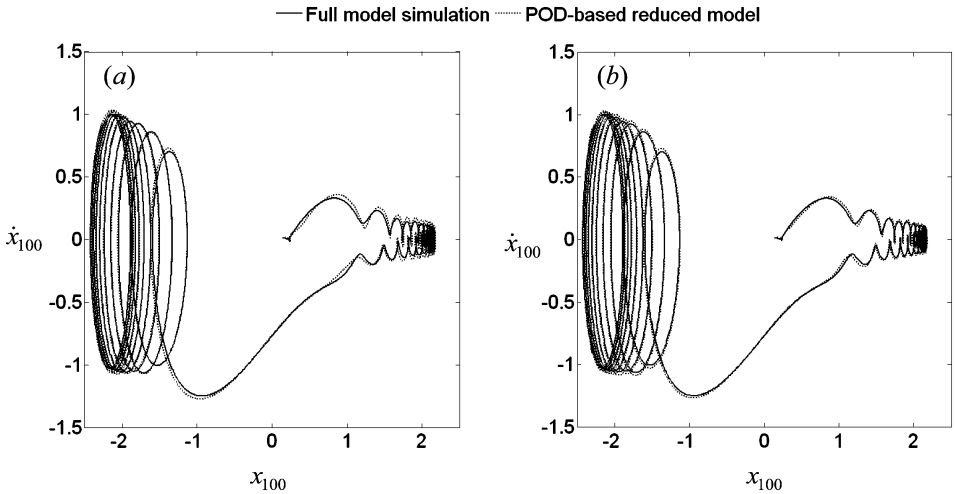

Fig. 14 Phase plane portraits of m_{60} obtained via numerical simulation of the full model and its reduced models up to $t = 100$ s: (**a**) 50 POMs, (**b**) 55 POMs

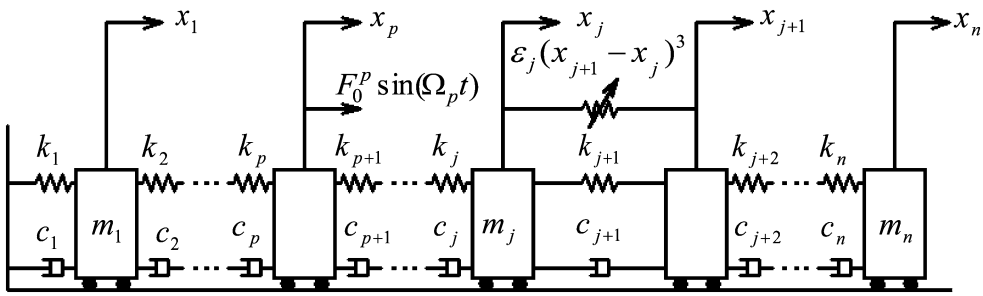

Fig. 15 The forced and damped n-degrees-of-freedom spring–mass system with coupling nonlinearity

As before, the LELSM requires setting all degrees-of-freedom to zero except those attached to the coupling spring as shown in Fig. 16.

For the parameter set $m_j = m_{j+1} = m, k_j = k_{j+2} = k, k_{j+1}$, and zero damping coefficients, the equations of motion of the system in Fig. 16 are simplified to

$$m\ddot{x}_j + (k + k_{j+1})x_j - k_{j+1}x_{j+1} + \varepsilon_j(x_j - x_{j+1})^3 = 0, \tag{24a}$$

$$m\ddot{x}_{j+1} - k_{j+1}x_j + (k + k_{j+1})x_{j+1} - \varepsilon_j(x_j - x_{j+1})^3 = 0. \tag{24b}$$

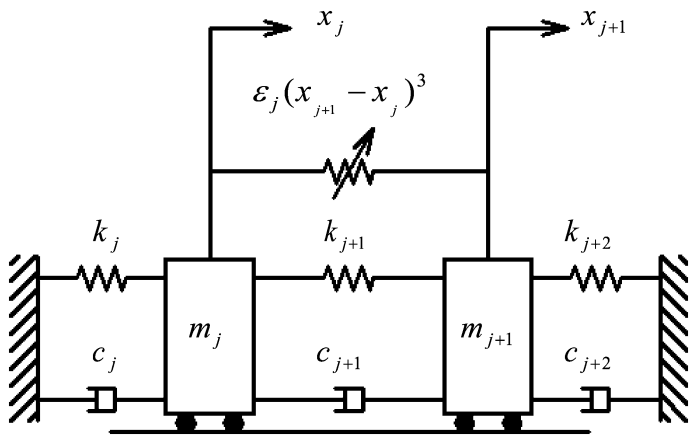

Fig. 16 The equivalent 2-degrees-of-freedom LELSM model of degrees-of-freedom j and $j+1$

Subtracting the second equation from the first one yields

$$m(\ddot{x}_j - \ddot{x}_{j+1}) + (k + 2k_{j+1})(x_j - x_{j+1}) + 2\varepsilon_j(x_j - x_{j+1})^3 = 0. \tag{25}$$

Letting $(x_j - x_{j+1}) = z_j$, (25) is simplified to

$$\begin{aligned} &\ddot{z}_j + \omega_{j0}^2\left(z_j + a_j z_j^3\right) = 0, \\ &\omega_{j0}^2 = (k + 2k_{j+1})/m, \\ &a_j = 2\varepsilon_j/(k + 2k_{j+1}). \end{aligned} \tag{26}$$

The frequency equation of the system in (26) is given as [34]

$$\Omega_j^2 = \frac{\omega_{j0}^2}{144}\left(80 + 62a_j Z_{j0}^2 + \sqrt{4096 + 5888a_j Z_{j0}^2 + 1684a_j^2 Z_{j0}^4}\right), \tag{27}$$

where $Z_{j0} = x_j(0) - x_{j+1}(0)$ is the initial amplitude of the system in (26) which can be rewritten in the following equivalent form:

$$\ddot{z}_j + \Omega_j^2 z_j = 0. \tag{28}$$

In addition, the system in Fig. 16 is assumed to be equivalent to the system in Fig. 17 of which the equation of motion in term of z_j is given by

$$m\ddot{z}_j + \left(k + 2(k_{\text{eq}})_j\right)z_j = 0. \tag{29}$$

Hence, from (28) and (29) the local equivalent stiffness is given by

$$(k_{\text{eq}})_j = \left(m_j\Omega_j^2 - k\right)/2. \tag{30}$$

For $n = 20$, $j = 15$, and unity stiffnesses and masses of the system with appropriate units, the same system as in [22] is considered here. The global stiffness matrix K is updated to K_{eq} as

$$K_{\text{eq}} = \begin{bmatrix} 2 & -1 & & & & & & \\ -1 & 2 & -1 & & & & 0 & \\ & \ddots & \ddots & \ddots & & & & \\ & & -1 & (1+k_{\text{eq}})_{15} & -k_{\text{eq}} & & & \\ & & & -k_{\text{eq}} & (1+k_{\text{eq}})_{16} & -1 & & \\ & 0 & & & \ddots & \ddots & \ddots & \\ & & & & & -1 & 1 & \end{bmatrix}. \tag{31}$$

By following the same iteration technique for grounded nonlinearities, the updated LELSM modes of this system are obtained.

The previously used K–B (Kumar–Burton) [22] and Milman–Chu [35] vectors with a system similar to that in Fig. 16 for enhancing the POD-based and linear-based reduced models are found to be efficient in enhancing the LELSM-based reduced model for such dynamic systems. These vectors are plotted in Fig. 18 where the vectors $r_{\text{k–b}}$ and $r_{\text{m–ch}}$ are calculated based on the use of the linear stiffness matrix while $\bar{r}_{\text{k–b}}$ and $\bar{r}_{\text{m–ch}}$ are calculated based on the use of the local equivalent linear stiffness matrix K_{eq}. The small difference between these vectors is made clear in Fig. 18. The use of K_{eq} in calculating $\bar{r}_{\text{k–b}}$ and $\bar{r}_{\text{m–ch}}$ was found to slightly enhance the order reduction over the use of the linear stiffness matrix for finding $r_{\text{k–b}}$ and $r_{\text{m–ch}}$. This enhancement can be seen only if the phase plane portraits are magnified.

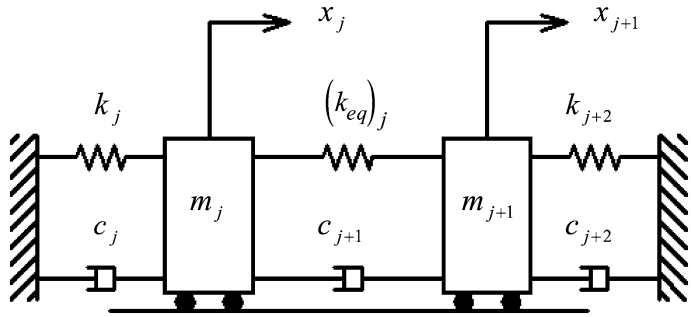

Fig. 17 The 2-degrees-of-freedom sub-system of the degrees-of-freedom j and $j+1$

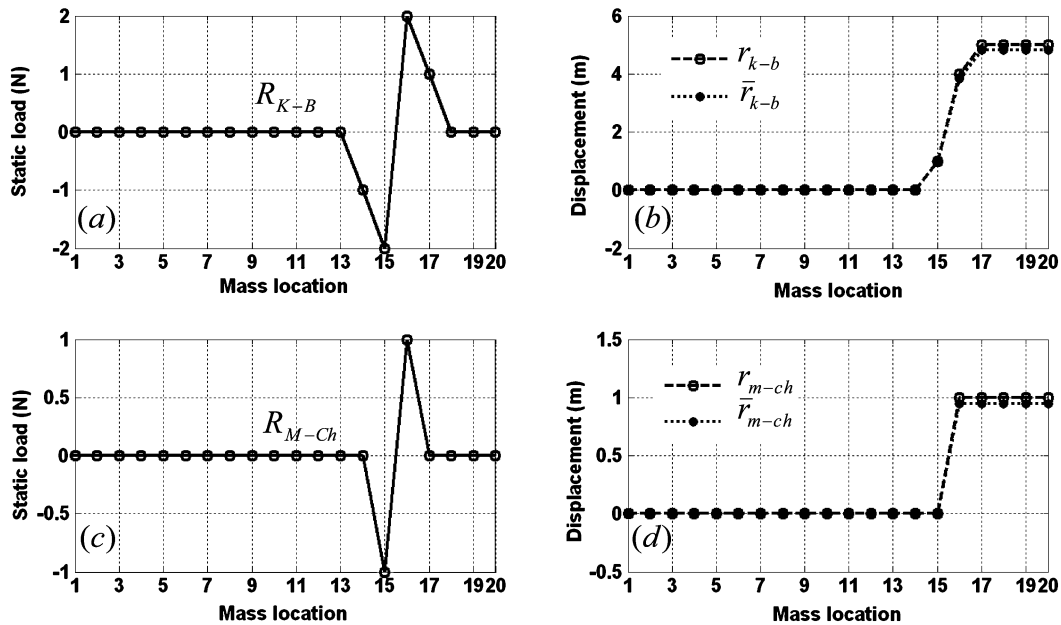

Fig. 18 Static load K–B and Milman–Chu vectors and their corresponding displacements of the masses of the 20-degrees-of-freedom system with forcing excitation at m_4 and cubic coupling spring attached between m_{15} and m_{16}: (**a**) and (**b**) K–B static load and displacement vectors, (**c**) and (**d**) Milman–Chu static load and displacement vectors

In the following example, the periodic excitation load with $F_0^4 = 5$ acts on m_4 and the cubic coupling spring is attached between m_{15} and m_{16} where $\varepsilon_{15} = 3$. The POD-based reduced models are plotted in Fig. 19. It is shown in this figure and in Table 6 that when the number of retained modes in the POD-based reduced model increased from 9 to 10, R_{POD} changes from 0.9980 to 0.9986. This does not actually reflect the considerable enhancement between the 9 POMs reduced model and the 10 POMs reduced model. Similarly to the nonlinear system with grounded nonlinearity, the R_{POD} is found here to not necessarily distinguish the minimum number of the retained modes to obtain a reduced order model of an acceptable accuracy.

The updated LELSM modes are augmented with one K–B and one Milman–Chu vector. It is found that the use of one K–B and one Milman–Chu vector with the updated LELSM modes gives a more enhanced reduced model than the same POMs. Unlike POD-based reduced model, a smooth enhancement in the LELSM-based reduced models is clear from Fig. 20 and from the accumulated least square error in Table 6. The enhanced LELSM-based reduced model is almost found to be more accurate than the POD-based and the linear-based reduced models for this example.

Table 6 Least square error '*LE*' between simulations of the full and the reduced models of m_{16}

Simulation time	500 seconds			
No. of modes retained	7	8	9	10
POD-based reduced model, $LE =$	2310	1069.3	771.2	391.9
LELSM-based reduced model, $LE =$	699.3	502.7	605.1	275.2
Linear-based reduced model, $LE =$	706.9	489.8	614.14	276
R_{POD}	0.9961	0.9971	0.9980	0.9986

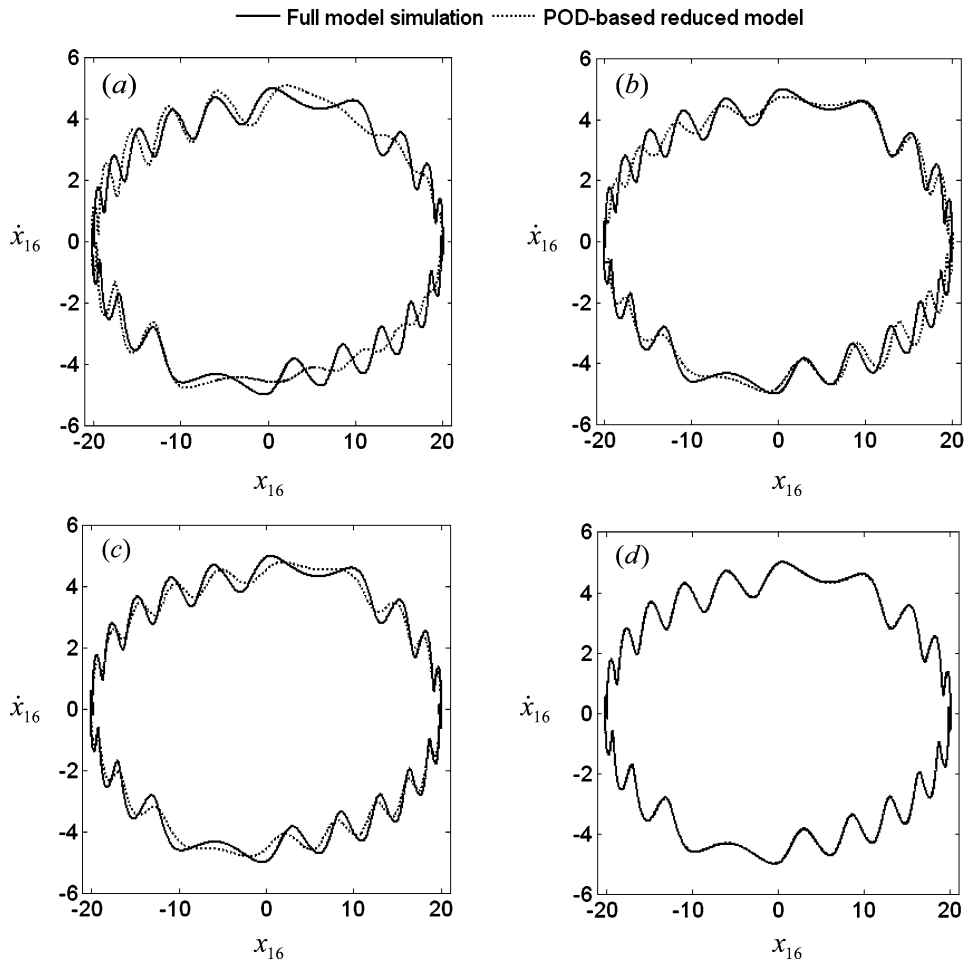

Fig. 19 Phase plane portraits of m_{16} obtained via simulation of the full and the reduced models of the forced nonlinear system with coupling nonlinearity: (**a**) 7 POMs, (**b**) 8 POMs, (**c**) 9 POMs, (**d**) 10 POMs

8 Conclusions

An order reduction technique for forced nonlinear dynamic systems with isolated nonlinearities is introduced in this paper. The technique is based on using a subset of the updated LELSM modes augmented to a subset of new Ritz vectors (Sh-B vectors). These new vectors are proportional to the stiffnesses of the masses attached to the forcing or nonlinear springs. Unlike in linear modes, the nonlinearity effect appears in these updated LELSM modes. These new modes preserve the nonlinear dynamics of the system. Hence, their augmentation with the Sh-B vectors in the modal order reduction transformation matrix for forced nonlin-

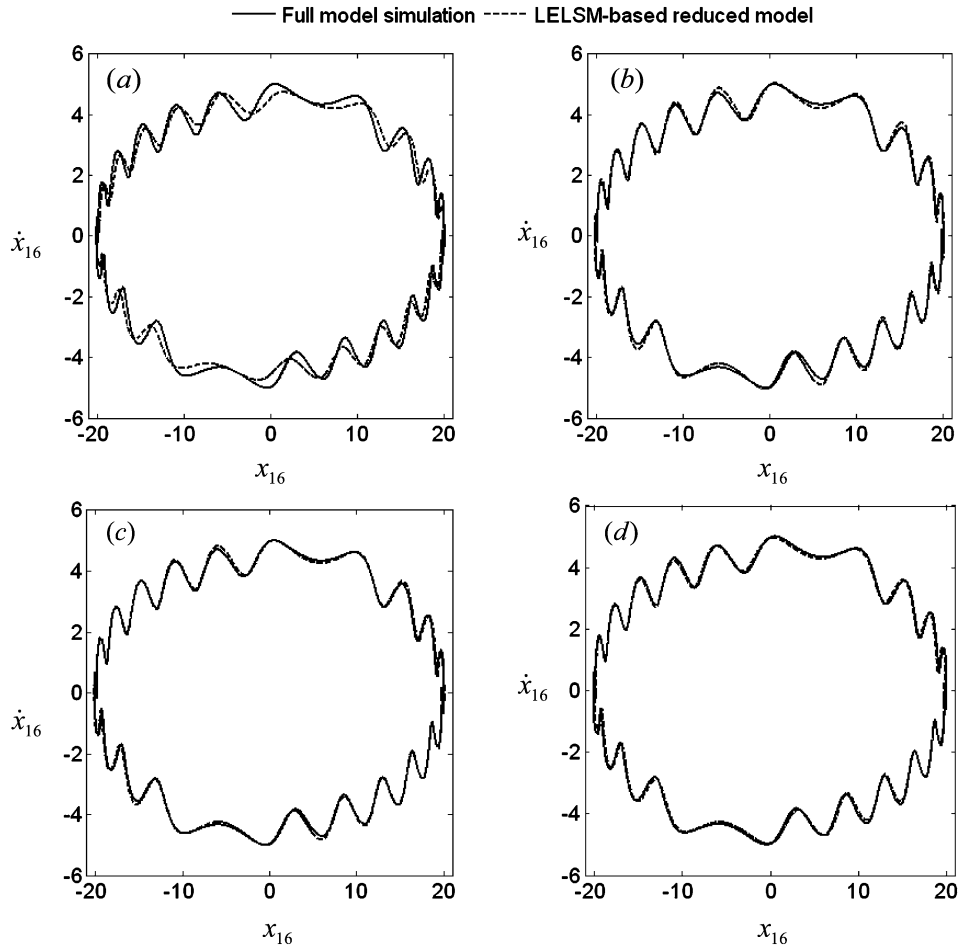

Fig. 20 Phase plane portraits of m_{16} obtained via simulation of the full and the reduced models of the forced nonlinear system with coupling nonlinearity: (**a**) 5 updated LELSM modes combined with one K–B and one Milman–Chu vector, (**b**) 6 updated LELSM modes combined with one K–B and one Milman–Chu vector, (**c**) 7 updated LELSM modes combined with one K–B and one Milman–Chu vector, (**d**) 8 updated LELSM modes combined with one K–B and one Milman–Chu vector

ear systems yields a reduced model that is comparable to the POD-based reduced model for all dynamic systems that are considered in this study.

The augmentation of the new Sh-B vectors with a subset of the updated LELSM modes was found to be as accurate as the use of a subset of POMs of the same dimension in reducing the order of a forced system with cubic nonlinearities. In addition, the exact frequencies of the nonlinear dynamic system with cubic stiffnesses are well approximated by the frequencies of the updated LELSM modes. The deviation between the frequencies of the updated LELSM modes and the linear modes allows for knowledge of the sensitivity of the modes to the nonlinear spring location. For the examples that are considered in this study, the high similarity between the POMs and updated LELSM modes is observed when the first linear mode is used as initial condition for such nonlinear systems. For the dynamic system with a coupling nonlinearity, the augmentation of the K–B and Milman–Chu vectors with a subset of the updated LELSM modes in the order reduction transformation matrix yields LELSM-based reduced model as efficient as the POD-based reduced model. Hence, Sh-B vectors were found to better enhance the LELSM-based reduced models of the forced systems with grounded nonlinearities while K–B and Milman–Chu vectors were found to better enhance the LELSM-based reduced models of forced systems with coupling nonlinearities.

It was found that the optimal locations of the displacements of the new Sh-B vectors are the masses which are connected to the nonlinear springs and forcing. The possibility of using more than two Sh-B vectors is demonstrated in this study via two large degrees-of-freedom systems with two cubic springs and one forcing. The results of these examples have shown that the use of three or more of the Sh-B vectors still produces a comparable LELSM-based reduced model to the POD-based reduced model. It is shown that the Sh-B vectors can be used for different locations of the nonlinear springs and forcing and yield comparable reduced models to POD-based reduced models. The main advantage of using the enhanced LELSM-based order reduction via a subset of the Sh-B vectors of the systems that are considered in this study is that, unlike POD-based order reduction, no a priori simulation of the full model is required and thus it can be applied directly to the model.

References

1. Guyan, R.J.: Reduction of stiffness and mass matrices. AIAA J. **2**, 380 (1965)
2. Burton, T.D., Young, M.E.: Model reduction and nonlinear normal modes in structural dynamics. In: Nonlinear and Stochastic Dynamics Symposium. AMD, vol. 192. DE, vol. 78, pp. 9–16. ASME Winter Ann. Mtg., Chicago, IL, pp. 6–11 (1994)
3. Friswell, M.I., Penny, J.E.T., Garvey, S.D.: Using linear model reduction to investigate the dynamics of structures with local nonlinearities. Mech. Syst. Signal Process. **9**(3), 317–328 (1995)
4. Burton, T.D., Rhee, W.: On the reduction of nonlinear structural dynamics models. J. Vib. Control **6**, 531–556 (2000)
5. Kim, J., Burton, T.D.: Reduction of structural dynamics models having nonlinear damping. ASME Paper no. DETC2003/VIB-48435
6. Butcher, E.A., Lu, R.: Order reduction of structural dynamic systems with static piecewise linear nonlinearities. Nonlinear Dyn. **49**, 375–399 (2007)
7. Shaw, S.W., Pierre, C.: Non-linear normal modes and invariant manifolds. J. Sound Vib. **150**, 170–173 (1991)
8. Jiang, D., Pierre, C., Shaw, S.: Large amplitude nonlinear normal modes of piecewise linear systems. J. Sound Vib. **272**, 869–891 (2004)
9. Peschek, E., Boivin, N., Pierre, C.: Nonlinear modal analysis of structural systems using multi-mode invariant manifolds. Nonlinear Dyn. **25**, 183–205 (2001)
10. Burton, T.D.: Numerical calculation of nonlinear normal modes in structural systems. Nonlinear Dyn. **49**, 425–441 (2007)
11. Shaw, S.W., Pierre, C., Pesheck, E.: Modal analysis-based reduced-order models for nonlinear structures—an invariant manifold approach. Shock Vib. Dig. **31**, 3–16 (1999)
12. Pesheck, E., Pierre, C., Shaw, S.W.: Modal reduction of a nonlinear rotating beam through nonlinear modes. J. Vib. Acoust. **124**, 229–236 (2002)
13. Sinha, S.C., Redkar, S., Butcher, E.A.: Order reduction of nonlinear systems with time periodic coefficients using invariant manifolds. J. Sound Vib. **284**, 985–1002 (2005)
14. Sinha, S.C., Butcher, E.A., Dávid, A.: Construction of dynamically equivalent time invariant forms for time periodic systems. Nonlinear Dyn. **16**, 203–221 (1998)
15. Feeny, B.F., Kappagantu, R.: On the physical interpretation of proper orthogonal modes in vibrations. J. Sound Vib. **211**(4), 607–616 (1998)
16. Feeny, B.F.: On proper orthogonal co-ordinates as indicators of modal activity. J. Sound Vib. **255**(5), 805–817 (2002)
17. Han, S., Feeny, B.F.: Enhanced proper orthogonal decomposition for the modal analysis of homogeneous structures. J. Vib. Control **8**(1), 19–40 (2002)
18. Lenaerts, V., Kerschen, G., Golinval, J.C.: Proper orthogonal decomposition for model updating of nonlinear mechanical systems. Mech. Syst. Signal Process. **15**(1), 31–43 (2001)
19. Kappagantu, R., Feeny, B.F.: An "optimal" modal reduction of a system with frictional excitation. J. Sound Vib. **224**(5), 863–877 (1999)
20. Kerschen, G., Golival, J., Vakakis, A., Bergman, L.: The method of proper orthogonal decomposition for dynamical characterization and order reduction of mechanical systems: an overview. Nonlinear Dyn. **41**, 147–169 (2005)
21. Kumar, N., Burton, T.D.: Use of random excitation to develop POD based reduced order models for nonlinear structural dynamics. In: Proceedings of the ASME IDETC, Paper DETC2007/VIB-35539, Las Vegas, NV, September 4–7 (2007)
22. Kumar, N., Burton, T.D.: On combined use of POD modes and Ritz vectors for model reduction in nonlinear structural dynamics. In: Proceedings of the ASME IDETC, Paper DETC2009-87416, San Diego, CA, September (2009)
23. Segalman, J.D.: Model reduction of systems with localized nonlinearities. J. Comput. Nonlinear Dyn. **2**, 249–266 (2007)
24. Kline, K.A.: Dynamic analysis using a reduced basis of exact modes and Ritz vectors. AIAA J. **24**(12), 2022–2029 (1986)
25. Balmès, E.: Optimal Ritz vectors for component mode synthesis using the singular value decomposition. AIAA J. **34**(6), 1256–1260 (1996)
26. Wilson, E.L., Yuan, M.W., Dickens, J.M.: Dynamic analysis by direct superposition of Ritz vectors. Earthquake Eng. Struct. Dyn. **10**, 813–821 (1982)
27. Lèger, P.: Application of load dependent vectors bases for dynamic substructure analysis. AIAA J. **28**(1), 177–179 (1990)
28. Hurty, W.C.: Dynamic analysis of structural systems using component modes. AIAA J. **3**(4), 678–685 (1965)
29. Craig, R.R., Bampton, M.C.C.: Coupling of substructures for dynamic analyses. AIAA J. **6**(7), 1313–1319 (1968)
30. Apiwattanalunggarn, P., Shaw, S.W., Pierre, C.: Component mode synthesis using nonlinear normal nodes. Nonlinear Dyn. **41**, 17–46 (2005)

31. Suy, H.M.R., Fey, R.H.B., Galanti, F.M.B., Nijmeijer, H.: Nonlinear dynamic analysis of a structure with a friction-based seismic base isolation system. Nonlinear Dyn. **50**, 523–538 (2007)
32. Butcher, E.A.: Clearance effects on bilinear normal mode frequencies. J. Sound Vib. **224**, 305–328 (1999)
33. Al-Shudeifat, M.A., Butcher, E.A., Burton, T.D.: Comparison of order reduction methodologies and identification of NNMs in structural dynamic systems with isolated nonlinearities. In: Proceedings of the International Modal Analysis Conference, Orlando, FL, February 9–12 (2009)
34. Belendez, A., Hernandez, A., Marquez, A., Neip, C.: Analytical approximation for the period of a nonlinear pendulum. Eur. J. Phys. **27**, 539–551 (2006)
35. Milman, H., Chu, C.: Eigenvalue error analysis of viscously damped structures using Ritz reduction method. AIAA J. **30**(12), 2935–2945 (1992)